Heliyon 8 (2022) e09830

Contents lists available at ScienceDirect

Heliyon

journal homepage: www.cell.com/heliyon

Research article

Accuracy of two dosimetry software programs for ^{177}Lu radiopharmaceutical therapy using voxel-based patient-specific phantoms

Keamogetswe Ramonaheng *, Johannes A. van Staden, Hanlie du Raan

Department of Medical Physics, Faculty of Health Sciences, University of the Free State, P.O. Box 339, Bloemfontein, 9300, South Africa

ARTICLE INFO

Keywords:
SPECT
Dosimetry
Accuracy
Monte Carlo
^{177}Lu-DOTATATE
OLINDA
LundADose
Radiopharmaceutical therapy
Patient-specific phantom
Voxel-based phantom

ABSTRACT

Purpose: Virtual dosimetry using voxel-based patient-specific phantoms and Monte Carlo (MC) simulations offer the advantage of having a gold standard against which absorbed doses may be benchmarked to establish the dosimetry accuracy. Furthermore, these reference values assist in investigating the accuracy of the absorbed dose methodologies from different software programs. Therefore, this study aimed to compare the accuracy of the absorbed doses computed using LundADose and OLINDA/EXM 1.0.

Methods: The accuracy was based on ^{177}Lu-DOTATATE distributions of three voxel-based phantoms. SPECT projection images were simulated for 1, 24, 96, and 168 h post-administration and reconstructed with LundADose using 3D OS-EM reconstruction. Mono-exponential curves were fitted to the bio-kinetic data for the kidneys, liver, spleen, and tumours resulting in SPECT time-integrated activity (SPECT-TIA). The SPECT-TIA were used to compute mean absorbed doses using LundADose (LND-D_{SPECT}) and OLINDA (OLINDA-D_{SPECT}) for the organs. Pre-defined true activity images, were used to obtain TRUE-TIA and, together with full MC simulations, computed the true doses (MC-D_{True}). The dosimetry accuracy was assessed by comparing LND-D_{SPECT} and OLINDA-D_{SPECT} to MC-D_{True}.

Results: Overall, the results presented an overestimation of the mean absorbed dose by LND-D_{SPECT} compared to the MC-D_{True} with a dosimetry accuracy $\leq$6.6%. This was attributed to spill-out activity from the reconstructed LND-D_{SPECT}, resulting in a higher dose contribution than the MC-D_{True}. There was a general underestimation (<8.1%) of OLINDA-D_{SPECT} compared to MC-D_{True} attributed to the geometrical difference in shape between the voxel-based phantoms and the OLINDA models. Furthermore, OLINDA-D_{SPECT} considers self-doses while MC-D_{True} reflects self-doses plus cross-doses.

Conclusion: The better than 10% accuracy suggests that the mean dose values obtained with LND-D_{SPECT} and OLINDA-D_{SPECT} approximate the true values. The mean absorbed doses of the two software programs, and the gold standard were comparable. This work shall be of use for optimising ^{177}Lu dosimetry for clinical applications.

1. Introduction

The recent development of novel radiopharmaceutical agents in the field of Nuclear Medicine (NM) has resulted in renewed interest in radiopharmaceutical therapy (RPT) and internal radiation dosimetry to evaluate the efficacy and toxicity of RPT. Different terminologies have been used to describe patient therapy using radioactive pharmaceuticals. However, the Society of Nuclear Medicine Molecular Imaging therapy task force survey has recently suggested using a consistent nomenclature for the field and recommends the term RPT to describe such a treatment [1], which is adopted in this work.

Lutetium-177 (^{177}Lu) has gained widespread interest and importance in RPT due to its decay properties. The radionuclide emits both gamma rays (predominantly with the energy of 208.4 keV and 112.9 keV) and beta particles with maximum energy of 498.3 keV (mean range in soft tissue of 0.7 mm) and has a physical half-life of 6.7 days [2]. Therefore, it can be used for therapeutic and imaging purposes since it has ideal properties for post-administration imaging, which allows patient-specific dosimetry. Neuroendocrine tumours (NETs) have been treated successfully using RPT, specifically peptide receptor radionuclide therapy (PRRT) with ^{177}Lu-DOTATATE [3, 4, 5, 6]. PRRT aims to irradiate tumour cells by coupling radionuclides such as ^{177}Lu to peptide molecules that bind to cell receptors. In some tumours these receptors may be over-expressed in abundance, allowing a high radiation dose to be delivered to the tumour cells. However, some non-tumour physiological uptake also occurs in organs such as the kidneys, liver, spleen, and bone

* Corresponding author.
E-mail address: BoomK@ufs.ac.za (K. Ramonaheng).

https://doi.org/10.1016/j.heliyon.2022.e09830
Received 27 October 2021; Received in revised form 18 February 2022; Accepted 24 June 2022

marrow. Thus, the radiation dose administered to the patient during PRRT (and RPT in general) is limited by the dose to healthy tissue (also referred to as organs at risk (OAR)). The effectiveness of RPT lies in the ability to deliver a lethal dose to the tumour cells while sparing the healthy tissue. PRRT with ^{177}Lu-DOTATATE has been well established in treating patients with late-stage NETs that overexpress somatostatin receptors. Trials have shown ^{177}Lu-DOTATATE to be an effective and well-tolerated form of treatment for NETs [7, 8, 9, 10]. Even though RPT (which includes ^{177}Lu-DOTATATE and ^{131}I-MIBG (meta-iodobenzylguanidine)) has been used for many years to treat NETs there is still much room to improve its patient-specific treatment efficacy.

Patient individualised therapy is a standard in treatment planning with external beam radiation therapy (EBRT), aiming to achieve better tumour control and less normal tissue toxicity. The same principle of individualised dosimetry-driven treatment planning is sought for RPT. The kidneys are recognised as the dose-limiting OAR for ^{177}Lu-DOTATATE PRRT because of the additional re-absorption by proximal tubules. Furthermore, Ilan et al. [11] have shown a significant correlation between tumour absorbed dose, tumour size, and tumour control for pancreatic NETs. It is thus valid, where possible, to extend dosimetry to the tumours. Similar to EBRT treatment planning, accurate knowledge of absorbed doses to both the tumour and normal tissue is advantageous in RPT treatment planning.

Since internal radiation dosimetry determines the amount of absorbed dose in tissue, the terms absorbed dose calculation and dosimetry shall be used interchangeably. For accurate patient-specific dosimetry, the bio-distribution and bio-kinetic data of the radiopharmaceutical is required to calculate the time-integrated activity (TIA) for each organ of interest. The total amount of radiation energy emitted by the radioactivity in each source organ is further required and known for the specific radionuclide used. The final parameter to include in the absorbed dose calculation is the fraction of energy emitted by each source organ and absorbed by the relevant target organs. Since this is dependent on the relative organ positions and sizes, patient-specific anatomical information is required.

Bio-kinetic data is patient-specific and emphasizes the validity of personalised dosimetry. The bio-kinetic data may be monitored with a gamma camera through patient-specific image-based quantification. The challenge for clinics and institutions is determining the best data collection method to quantify bio-kinetic data for different tissue regions. Clinics have adopted different image acquisition and data processing protocols [12]. According to Bardiès and Gear [13], dosimetry is a component of a clinical workflow chain that includes the following steps: patient data acquisition, gamma camera calibration, activity quantification, image registration and segmentation, time-activity curve (TAC) fits and absorbed dose calculations. Although commercial software applications are available to perform dosimetry, not all aspects of the chain are always included on par with one another. Thus, there is always a need to optimize these applications [14]. The dosimetry's image acquisition and processing methods are predominately dependent on a clinic's accessibility and acquaintance with dosimetry software. SPECT/CT is promoted as part of a clinical workflow. However, using SPECT data to determine absorbed dose estimates is protocol-dependent and has method-specific limitations.

The demand for patient-specific image-based dosimetry treatment planning necessitates developing clinically feasible dosimetry protocols. Patient-specific dosimetry entails using patient bio-kinetic data and anatomy to perform the dose calculations. Although more accurate, it is also laborious [15]. Currently, the approach to clinical dosimetry is two-fold: One, it may be patient-specific, or two, model-based, where the former is known to be more accurate and the latter easier and faster to implement routinely. There is a trend to move from model-based to patient-specific dosimetry to improve the accuracy of absorbed dose calculations [16, 17, 18].

The standard method used for absorbed dose calculations, which has gained wide acceptance in NM, is the Medical Internal Radiation Dose (MIRD) formalism [19, 20]. The MIRD method calculates the mean absorbed dose $\overline{D}(r_T, T_D)$ delivered to the target organ r_T over a defined dose-integration time T_D (from 0 to ∞) after administering a radionuclide, expressed as Equation (1):

$$\overline{D}(r_T,\ T_D) = \sum_{r_S} \tilde{A}(r_s, T_D).S(r_T \leftarrow r_S) \tag{1}$$

where $\tilde{A}(r_s)$ is the time-integrated activity (TIA) (also referred to as the cumulated activity, i.e., the total number of nuclear decays) in the source organ r_S, $\sum_{r_S}$ denotes the contribution of several source organs, $S(r_T \leftarrow r_S)$ is the mean absorbed dose delivered to the target organ r_T per unit cumulated activity in the source organ, is also known as the S value. The S value is radionuclide specific since it depends on the energy and yield of each nuclear transition. In essence, the absorbed dose calculations are the product of TIA with the S values, and the dosimetry accuracy relies on these two terms.

The TIA depends mainly on the image quantification methods and their accuracy. Apart from the activity quantification accuracy, the accuracy of TIA depends on the number of consecutive imaging time-points post-administration, the frequency of the imaging time-point, the appropriate imaging time-span after administration (integration period), and the integration of these time-points, i.e., the model used to fit the TAC before integration [21, 22, 23]. The results used to calculate the absorbed doses are usually presented either as TIA (MBq.s) or the residence time (s) defined as TIA normalised to the activity (MBq) administered to the patient.

The S value, the second important factor in absorbed dose calculations, may be determined from computed pre-calculations based on reference models [24, 25, 26] and radiation transport algorithms. These algorithms are subdivided into local energy depositions (LEDs) [27, 28], convolution with dose-voxel kernels [29, 30], and full MC-based radiation transport calculations [31, 32, 33, 34, 35]. Although the LED method is the simplest, it may be limited in accuracy and valid only for non-penetrating radiation particles such as alpha's, beta's, and Auger electrons [36]. The LED method assumes that all the radiation energy is deposited within the respective voxel. Since most radiation-charged particles used in RPT have a path length less than the voxel dimensions of the reconstructed SPECT activity image, the assumption is valid [34]. It falls short when the gamma radiation is emitted with a high yield and an increased cross-dose contribution [37, 38]. The convolution with the dose-voxel kernels method assumes each voxel to have a uniform source distribution [29, 39] and computes voxel S values for a specific radionuclide, tissue density, and voxel dimension using MC transport [30, 40]. The distinct advantage of MC-based calculations is the ability to take non-homogeneous activity distribution into account. Furthermore, MC-based dosimetric calculations account for patient-specific geometry, the transition between tissue types, and the induction of secondary particles [30, 41]. Full MC-based radiation transport calculations are justified when the radiation range exceeds the spatial resolution of the image from which the absorbed dose is calculated, hence, it may not always be warranted for reconstructed SPECT images [38]. The approach to choosing the appropriate radiation transport algorithm depends on the radiation range, the imaged geometry, and the gamma camera's spatial resolution assuming that the activity is quantified accurately for the given spatial resolution. As a rule of thumb, LED may be used for non-penetrating radiation, while convolution-based and full MC transport algorithms may be intended for penetrating radiation in homogeneous and non-homogeneous geometries, respectively [13]. Ljungberg and Sjögreen Gleisner [34] have reported their institution-specific dosimetry software program, LundADose [38, 42], to accurately calculate absorbed doses for voxel dimensions used in clinical SPECT images, assuming the kinetic energy from charged particles (electrons) is locally absorbed. The assumption holds true, based on the poor spatial resolution of the SPECT images used as input for dosimetry which is comparable to or larger than the projected maximum range of the electrons. ^{177}Lu emits gamma radiation (208.4 keV) with low yield (10.4%) and thus has negligible cross-dose contribution [43].

In the last few years, gamma camera manufacturers or independent companies have created many dosimetry software programs using the algorithms mentioned above. The accessibility of the dosimetry software programs is determined by whether they are commercial or academic, have Food and Drug Administration (FDA) approval, are well maintained and documented, and are available in the public domain. Commercial dosimetry software programs available for clinical use, including the European CE marking, are summarised in Table 1.

The dosimetry software programs mentioned above are limited to some clinics due to a lack of affordability. For this reason, OLINDA/EXM 1.0 [26], which shall further be termed OLINDA, is still the most widely adopted dosimetry software program. Additionally, research institutions and clinics become resourceful in obtaining in-house developed dosimetry software, which strives to encompass most, if not all aspects, of the clinical dosimetry workflow. One such software program is LundADose. LundADose and OLINDA shall be used in this work and are discussed in Sections 2.2 and 2.3, respectively.

A comparison of the estimated absorbed doses for dosimetry from ^{177}Lu-DOTATATE by some authors is shown in Table 2. It can be noted from Table 2 that most of the authors applied the SPECT/CT or the hybrid WB/SPECT imaging method to perform the dosimetry. The number of subjects was mainly based on patients who underwent ^{177}Lu-DOTATATE treatment in the respective clinics. The dosimetry was tailored to be personalised by using patient-specific bio-kinetic data and varied between the authors. The studies listed in Table 2 demonstrate variations in absorbed dose estimates for critical organs such as the kidneys. This variation is caused by the differences in methods used in the clinics. As a result, dosimetry with ^{177}Lu-DOTATATE remains an ongoing investigation for many clinics with scope for optimising the methods. Due to these reported variations, an investigation into the accuracy of the dosimetry calculations becomes an important factor to consider. Only a limited number of studies have performed virtual absorbed dose calculations based on MC simulated gamma camera images of clinically realistic voxel-based patient-specific phantoms [45]. The results of such a study have the advantage of having a reference value (gold standard) to which the absorbed doses can be compared, which may be challenging to establish in a clinical setting.

Therefore, we aimed to compare the accuracy of ^{177}Lu absorbed doses computed using LundADose and OLINDA with reference MC true doses in voxel-based patient-specific phantoms.

2. Materials and methods

2.1. Monte Carlo simulations

The MC simulation software program SIMIND (SIMIND version 6.1.2 [55], validated in our previous work [56], was used in this study. We created a model of the Siemens Symbia T16 hybrid SPECT/CT gamma camera (Symbia T16) (Siemens Medical Solutions, Inc. Hoffman Estates, IL., USA), which was used to mimic ^{177}Lu gamma camera performance characteristics successfully. In the current work, we created three individual voxel-based clinically realistic phantoms, shown in Figure 1, identified as two females and a male. Due to the unavailability of ^{177}Lu-DOTATATE patient data in our clinic, the phantoms were created from anonymised liver-spleen SPECT/CT patient datasets obtained from the Symbia T16 database at Universitas Academic Hospital in Bloemfontein, South Africa. This study was approved by our institution's ethics committee in accordance with the Declaration of Helsinki and the radiation control committee. The voxel-based patient phantoms were created by segmenting the CT images of the patients using ITK-snap [57]. Each segmented region for the kidneys, liver, spleen, tumours, and the remainder of the body, was assigned a unique value to represent the different organs, generating an activity source map. The method followed to create the voxel-based patient phantoms, and the details of the simulation protocol are discussed in our preceding publications [56, 58].

This work represents the third contribution from our group concerning the accuracy of ^{177}Lu SPECT activity quantification and patient-specific dosimetry using MC simulations. The current study was designed to investigate the dosimetry accuracy, i.e., the last step in the absorbed dose calculation chain, for the two software programs mentioned above. For this reason, the data simulation, processing, and SPECT image activity quantification method extend from our previous work [58]. The same methodology was followed to determine the voxel-based patient phantoms' calibration factor (CF) and SPECT activity quantification. We demonstrated that comparable SPECT quantification accuracies were obtained between sphere and cylinder CFs when their corresponding recovery coefficients (RCs) were used for partial volume correction (PVC) [58]. We opted for the sphere CF in the current study due to its more practical clinical implementation.

The patient-specific bio-kinetic data (TIA activity concentration values for the OAR and tumours) was based on ^{177}Lu-DOTATATE bio-kinetic distributions reported by Brolin et al. [49] shown in Figure 2. Brolin et al. [49] used three pharmacokinetic digital phantoms from the XCAT generation to assess the dosimetry accuracy of ^{177}Lu-DOTATATE RPT. Similarly, we used three voxel-based patient phantoms to investigate the ^{177}Lu dosimetry accuracy for the OAR pertinent to ^{177}Lu-DOTATATE, namely the kidneys, liver, spleen, and the tumours. The same bio-kinetic data was used for all three phantoms. The use of spheres to mimic tumours is well established [59]. Therefore, two spheres of volume 33.5 ml (with a corresponding diameter 4.0 cm) were positioned adjacent to the liver (tumour-LV) and between the lungs (tumour-LNG). The organ and tumour concentrations of the three phantoms were based on the administered activity of 5533 ± 1850 MBq [17, 60] during the simulation and were kept the same for the three phantoms.

Table 1. Commercial dosimetry software programs with CE marking available for clinical use.

Dosimetry software	Imaging methods	Dosimetry method	Manufacturer	Reference
QDOSE ®	Planar, SPECT/CT, hybrid WB/SPECT	Convolution	ABX-CRO advanced pharmaceutical services Forschungsgesellschaft Germany	https://www.quantitativedose.com/ [44]
PLANET® Onco Dose (PDOSE)	SPECT/CT, hybrid WB/SPECT	LED convolution	DOSIsoft SA, Cachan, France	https://www.dosisoft.com/products/planet-dose/
MIM SurePlan™ MRT	SPECT/CT, hybrid WB/SPECT	Convolution	MIM Software Inc. Cleveland. OH, USA	https://www.mimsoftware.com/nuclear_medicine/sureplan_mrt
Dosimetry Toolkit®	Planar, SPECT/CT, hybrid WB/SPECT	OLINDA/EXM 1.0 and 2.0	GE healthcare, Waukesha, WI, USA	https://www.gehealthcare.com/products/molecular-imaging/nuclear-medicine/xeleris-4-dr
Hybrid Dosimetry Module™ (HDM)	Planar, SPECT/CT, hybrid WB/SPECT	OLINDA/EXM 2.0 and MC method	HERMES medical solutions, Stockholm, Sweden	https://www.hermesmedicalsolutions.com/organdosimetry/ [24]

LED, Local energy deposition; *MC*, Monte Carlo; *hybrid WB/SPECT images*, hybrid planar whole-body SPECT/CT images.

Table 2. A comparison of published mean absorbed doses for dosimetric analysis of ^{177}Lu-DOTATATE distribution.

Organ	Image method	Dosimetry method	Number of subjects	Mean Dose range (mGy/MBq)	Reference
Kidneys					
SPECT/CT		MC transport	21	0.90 ± 0.21	[46]
SPECT/CT		OLINDA/EXM 1.0	47	0.55–1.15	[47]
SPECT/CT		MIRD-dosimetry	20	0.34 ± 1.16	[48]
Hybrid-WB/SPECT		OLINDA/EXM 1.0 and MC transport	3 XCAT phantoms	2.98–4.34	[49]
SPECT/CT		OLINDA/EXM 1.0	777	0.5–13.1	[50]
Liver					
SPECT/CT		OLINDA/EXM 1.0	12	0.54 ± 0.58	[51]
SPECT/CT		DTK, HDM, Stratos, PDOSE, MIM	2	1.28 ± 1.25	[14]
Hybrid-WB/SPECT		OLINDA/EXM 1.0 and MC transport	3 XCAT phantoms	1.66–1.69	[49]
Spleen					
SPECT/CT		DTK, HDM, Stratos, PDOSE, MIM	2	0.7 ± 0.92	[14]
SPECT/CT		OLINDA/EXM 1.0	61	1.17 ± 0.14	[52]
Hybrid-WB/SPECT		MIRD-scheme	41	1.5–10.6	[53]
Tumour					
SPECT/CT		Full MC-transport	5	5.20–42.60	[16]
SPECT/CT		LED from SPECT	7	0.10–20.00	[46]
Hybrid-WB/SPECT		MC transport	180	2–77	[54]

MC, Monre Carlo*; DTK*, Dosimetry Toolkit® from GE-OLINDA/EXM 1.0; *HDM*, Hybrid dosimetry module™ from HERMES (v1)-OLINDA/EXM 2.0; *Stratos,* from Phillips-convolution; *PDOSE,* PLANET® Onco Dose from DOSIsoft (v 3.1.1)-local energy deposition convolution.

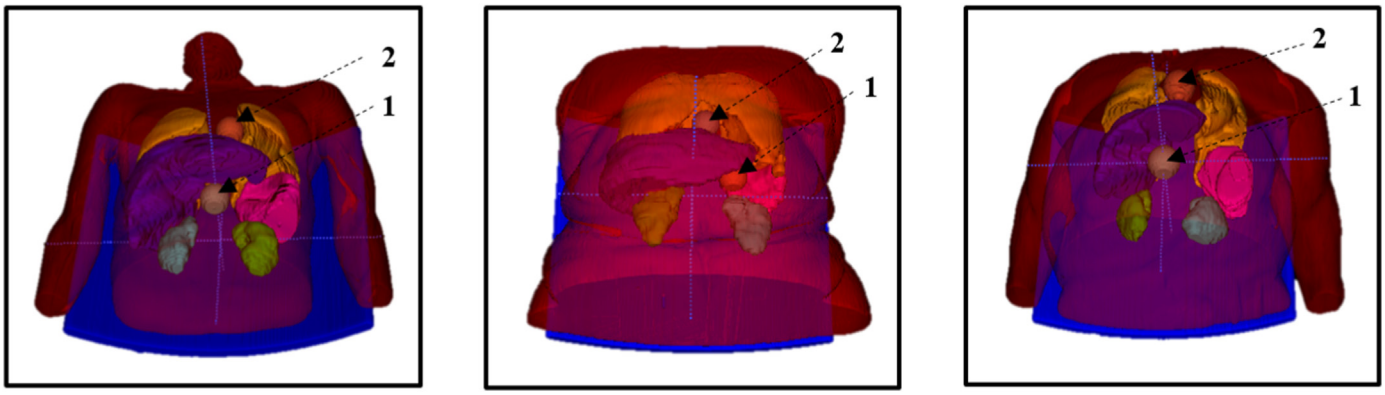

Figure 1. Three voxel-based patient-specific phantoms segmented using CT data fitted with spheres representing tumours. The arrows indicate sphere positions 1 and 2, representing tumours adjacent to the liver (tumour-LV) and between the lungs (tumour-LNG).

Simulations were performed for the ^{177}Lu 208.4 keV photopeak and 20% centred energy window, using a medium-energy (ME) collimator. Sixty projections were simulated with an equivalent acquisition time of 45 s per projection in a 128 × 128 image matrix with a pixel size of 4.8 × 4.8 mm^2. SPECT projections were simulated for imaging time-points 1, 24, 96, and 168 h post-administration. More than 1 billion photon

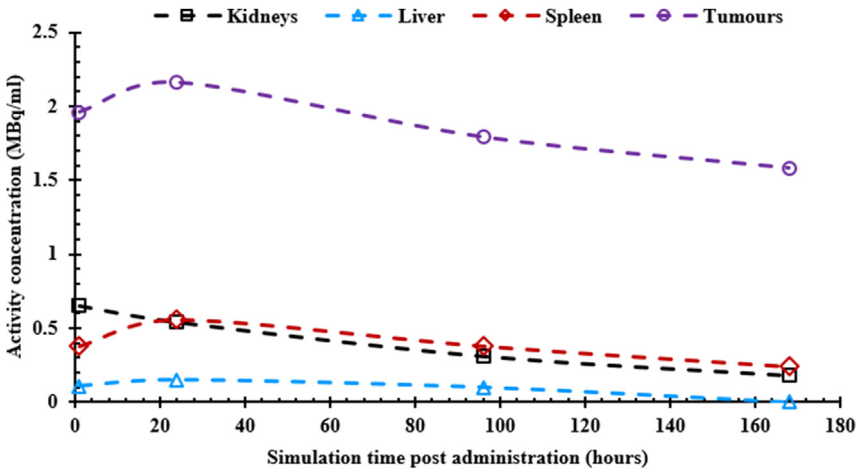

Figure 2. Bio-kinetic activity concentration distribution data used to simulate SPECT projections for four imaging time-points post-administration.

histories/projection were used for all simulations to ensure low simulation noise in the datasets [61].

The challenge for a comparative study such as ours, as indicated by Mora-Ramirez et al. [14], who compared five commercial dosimetry software programs in patients treated with ^{177}Lu-DOTATATE, is that the software programs do not all address the same steps in the clinical dosimetry workflow chain. In addition, the data handling in each part of the chain may be different for each software program, which complicates the comparative exercise and entails evaluating the uncertainties in each step. OLINDA has been developed to automate and standardise absorbed dose calculations for NM applications. It has also served well as a teaching tool and has practically facilitated comparisons between clinics. The LundADose software program was accessible to our group through research collaboration. To allow a fair comparison of the two software's dosimetry sections, we found it reasonable to have a checkpoint for the accuracy only at the absorbed dose calculation step. Contrary to OLINDA, LundADose included all steps in the dosimetry workflow chain and allowed standard criteria for input data prior to the absorbed dose calculations. Therefore, the TIA was computed using LundADose, as explained below, and thereafter the absorbed dose estimates were computed using LundADose and OLINDA.

2.2. LundADose

LundADose was developed in-house by the Department of Medical Radiation Physics, University of Lund, Lund, Sweden. The software program was initially written using the EGS4 code system [62] for MC particle simulation of the electron and photon transport and, for the most part, has since been replaced by the updated version EGSnrc program [32]. The MC-based absorbed dose calculations, together with the patient CT and SPECT data, can be used for patient-specific dosimetry. The reconstructed SPECT image is used to estimate the activity distribution during the transport modelling (particle tracking). Assuming that each voxel value reflects the activity distribution corresponding to the voxel location within the patient, the program can sample the decay of the particles through the radionuclide-specific decay scheme. The particle tracking and energy deposition (from appropriate interactions) is done through a density map derived from the patient CT data. The result is a 3-D dose map of absorbed dose rate with the same dimensions as the reconstructed SPECT image [63]. Apart from the absorbed dose calculations, LundADose also incorporates all other steps in the clinical dosimetry chain. The interface is written and developed in Interactive Data Language and calculates image-based absorbed doses using either planar whole-body, SPECT/CT, or hybrid WB/SPECT images. It incorporates methods for SPECT reconstruction with complete corrections, including image registration [64]. The program follows the photons by full MC transport to include the cross-doses between organs.

2.2.1. True dose image

2.2.1.1. Full Monte Carlo transport. MC transport modelling is considered the gold standard for calculating absorbed doses [42]. Therefore, the accuracy of the mean absorbed doses from the reconstructed SPECT dose images (discussed in Section 2.2.2) of the patient phantoms were benchmarked against the true MC absorbed doses (MC-D_{True}). The MC-D_{True} were determined from a true dose image with full MC transport, described below. The true dose image was created directly from the pre-defined activity source map and the aligned density map of the voxelized patient phantoms. The source map contained unique values of the segmented organs [56] for the kidneys, liver, spleen, lungs, tumour, and the body's remainder. Using ImageJ (Fiji) [65] the source map was scaled to a 128 × 128 image matrix, and the organ indexes were assigned the radioactive concentration values defined in the simulation. These images represented the true activity maps, excluding the degradation induced by the imaging and reconstruction processes.

The true activity images were used to calculate the True-TIA and entered into LundADose. The organ delineation part of the software program allowed the user to define volumes of interest (VOIs) from the segmented images based on the CT data. The VOIs for the kidneys, liver, spleen, and tumours were delineated according to the physical borders of the CT data, and each organ VOI file was saved. The true SPECT images of the four time-points were analysed using the saved VOI files. The program sums the activity concentration within each segmented volume of the different organs. The VOIs were superimposed onto each organ's four time-points, generating a TAC (MBq vs. hr). A mono-exponential curve [3, 49, 66, 67] was fitted to the TAC, generating a result file with True-TIA (MBq. hr) for each organ. The mean absorbed dose estimates were computed utilising full MC transport by incorporating phantom-specific density map information generated from CT data and the phantom true activity SPECT data.

The absorbed dose calculations for *full MC transport* incorporated in LundADose [42] used the EGS4 and EGSnrc programs to calculate the three phantoms' S values. The program used "all" particles' interaction of matter with photons, electrons, and beta particles, which includes spatial energy deposition scoring and sampling of decay positions [68]. The MC transport incorporated patient-specific anatomical information from the density map and the activity distribution obtained from the true SPECT data. The code generates cross-sections for lung, soft tissue, and bone normalised to a unit density. The voxel mass density is multiplied with the appropriately normalised cross-section to obtain the voxel cross-sections during the simulation. The transport simulation cut-off energies for which each history was terminated and the energy deposited were 0.01 MeV and 0.1 MeV for the photons and electrons, respectively. Subsequently, the energy deposition in all structures was scored and divided by the respective region mass. All simulations were performed with an adequate number of histories (100 million histories). The cut-off energy and number of histories were selected to ensure reasonable simulation time while maintaining low statistical uncertainty. The true activity images used with full MC transport to compute the absorbed doses as described above resulted in the MC-D_{True}.

2.2.1.2. Local energy deposition. Because the LED assumption within a voxel for the energy delivering electrons simplifies SPECT/CT dosimetry and holds true for most radionuclides used for RPT, it was acceptable to calculate the true doses using the same assumption. Even though MC is the gold standard, it is justified when the range of the particle under investigation is larger than the voxel size of the SPECT/CT image [38], which is not the case for ^{177}Lu. Furthermore, full MC dosimetry calculations can be computationally intensive and have not been entirely adopted in routine clinical applications. Therefore, the true doses were additionally computed for this study, assuming LED self-dose from electrons.

Similar to the MC-D_{True}, the phantom-specific density map and true activity images were incorporated, and the LED was computed as follows. LundADose was used to compute the average absorbed dose, assuming the LED from electrons is absorbed in the respective voxel. The emitted electron energy was weighted by the yield and summed over all electron energies resulting in the total energy emitted per decay. This assumption serves as reasonable since for ^{177}Lu the electron dose is completely dominant due to the low photon yield. The aligned density map for each patient was converted to a mass image. The absorbed dose was calculated by curve fitting and numerical integration, multiplying the TIA by the emitted energy per decay. Further on, the mean absorbed dose rate was computed by dividing the rate of absorbed energy with the corresponding mass taking into account the voxel dimensions, resulting in the absorbed dose rate per voxel. The dose computed from the LED of electrons using the true activity images shall be termed e-D_{True}

2.2.2. Reconstructed SPECT dose image

The simulated SPECT projections of the voxel-based patient phantoms obtained with SIMIND were reconstructed in LundADose using the 3D ordered subset expectation maximization (OS-EM) algorithm with pre-

determined optimal OS-EM updates (80 updates) [58]. The 3D OS-EM algorithm incorporated a CT-based attenuation correction, effective source scatter estimation scatter correction, and a collimator detector response correction [69, 70]. Appropriate PVC was applied using previously determined RCs for the tumours, and partial volume was corrected for the kidneys and spleen as described in Ramonaheng et al. [58]. Using ImageJ, the reconstructed activity images were compensated for partial volume by numerically correcting each segmented region with an appropriate RC. Similar to the true SPECT images the reconstructed images were entered into LundADose, and the mean absorbed doses were computed using full MC transport (as described in Section 2.2.1.1) and shall be termed LND-D_{SPECT}.

2.3. OLINDA

OLINDA (version 1) was used in this work due to its availability in our institution. OLINDA allows the user to input TIA per administered activity to calculate the mean absorbed organ doses. The adult male or female OLINDA models were appropriately selected for ^{177}Lu. The results obtained using LundADose, up until and including the fitting of TIA data, were transcribed to OLINDA to represent the kinetic input data. The TIA obtained from LundADose was normalised to the total activity used in the simulation, and target organ doses were calculated using OLINDA. Instead of using specific S values calculated using full MC transport for the voxel-based patient phantoms (LND-D_{SPECT}), each simulated patient organs' total doses were computed using the pre-computed S values from the OLINDA models [26]. The target organ S values (Vanderbilt University, Nashville, Tennessee, USA) (for self-irradiation) were scaled appropriately to the respective masses of the voxelized patient phantoms' organs as defined by the VOIs obtained from the CT data. The sphere sub-nodule was used to calculate the tumour absorbed doses, modelled as unit-density spheres of mass 33.6 g, estimating the absorbed dose to this volume. Although it is possible to calculate self-dose plus cross-dose contribution to the target organ using OLINDA, it is in most cases generally used and accepted to calculate only self-dose from the target organ for RPT. Furthermore, OLINDA does not account for cross-dose to and from the tumours. For this reason, it seemed meaningful to explore the e-$D_{True,}$ which accounted only for self-dose in the true dose images.

2.4. Evaluation of dosimetry accuracy

The main aim of this work was to determine the accuracy of the mean absorbed dose estimates from LND-D_{SPECT} and OLINDA-D_{SPECT} with reference to the MC-$D_{True.}$ This was achieved by calculating the dosimetry accuracy of three voxel-based patient-specific phantoms for ^{177}Lu-DOTATATE distribution in the kidneys, spleen, liver, and tumours. The measure of error, termed the accuracy, was represented as a percentage difference between the mean SPECT estimates *(SPECT)* and the true estimates *(TRUE)*, as shown in Equation (2).

$$Accuracy\ (\%) = \frac{SPECT - TRUE}{TRUE} \times 100 \quad (2)$$

The accuracy evaluation was extended and essentially evaluated fourfold for:

(i) SPECT-TIA versus True-TIA
(ii) LND-D_{SPECT} versus MC-D_{True} (self-dose and cross-dose)
(iii) OLINDA-D_{SPECT} versus MC-D_{True} (self-dose and cross-dose)
(iv) OLINDA-D_{SPECT} versus e-D_{True} (self-dose)

It should be noted that *SPECT* (Equation 2) appropriately represented the SPECT-TIA, LND-D_{SPECT} or OLINDA-D_{SPECT} while *TRUE* represented True-TIA, MC-D_{True} or e-D_{True} depending on the comparison (i-iv), which shall be stipulated accordingly. Where appropriate, the absolute differences between the average values shall be reported. The evaluation of the dosimetry accuracy is illustrated in Figure 3.

3. Results

3.1. Time-integrated activity accuracy

Using data obtained for voxel-based patient phantom 2, an example of the typical TACs obtained from the three patient phantoms for the four time-points at 1, 24, 96, and 168 h of the reconstructed SPECT images are shown in Figure 4. The best-fitting function available with LundADose for the curves was evaluated by visual inspection, a method previously adopted by other authors [71]. Mono-exponential fits were the best model to describe the progression of the activity in the source VOIs for the organs of interest, including the tumours. Brolin et al. [49], whose bio-kinetic data was adopted in this study, also used this fitting function. A slight deviation from the fitting function was observed at 96 and 168 h for the tumor data. Except for the kidneys, all the organs of interest exhibited a two-phase TAC characterised by a rapid activity uptake followed by a slower washout phase. The kidneys exhibited a single-phase curve with a more rapid washout phase in comparison to the other organs. In addition, co-registered true activity images and reconstructed SPECT images indicating VOIs for the kidneys, spleen and tumour-LNG are shown in Figure 5.

The TIA was calculated using the true activity images (True-TIA) and the reconstructed SPECT (SPECT-TIA) images and computed in LundADose by fitting the mono-exponential model to the data obtained for the four time-points (Figure 4). The average TIA data and associated standard deviation of the three patient phantoms for the kidneys, spleen, liver, and tumours are presented in Figure 6.

The SPECT-TIA slightly overestimated the TRUE-TIA. The error bars were calculated as one standard deviation obtained from the results of the three phantoms. On average, comparable values were obtained between the TRUE-TIA and SPECT-TIA for the respective organs with less than 5% percentage differences.

Since the mean absorbed doses for LundADose and OLINDA were calculated using SPECT-TIA data, it was worth comparing the accuracy between the TRUE-TIA and the SPECT-TIA for the three patients, summarised in Table 3.

The accuracy of the SPECT-TIA for all organs considered was in the range 1.3–7.2%, with the largest percentage difference obtained for the spleen of phantom 2 (Table 3). The average accuracy was calculated for the respective organs between the phantoms (inter-phantom) and between the organs for a particular phantom (intra-organ) to show variability. A slightly higher inter-phantom variability ($\leq 4.6 \pm 2.2\%$) was observed compared to the intra-organ variability ($\leq 3.8 \pm 1.8\%$). Overall the accuracy between the TRUE-TIA and SPECT-TIA was less than 7.2%.

3.2. Mean absorbed dose accuracy

The mean absorbed doses computed in LundADose by full MC transport using the true activity images (MC-DTrue) and fitting mono-exponential functions, were compared to the mean absorbed doses from the reconstructed SPECT images fitted to the same function calculated in LundADose (LND-DSPECT) and OLINDA (OLINDA-DSPECT), and presented demographically in Figure 7. As mentioned above, the e-DTrue estimates are presented because they carry a similar assumption to OLINDA (self-dose from target) and at the same time offer the opportunity to assess the contribution of the MC cross-dose. The overall trend of the mean absorbed doses, with the largest doses in the tumours, followed by the spleen, kidneys, and liver, was observed by other authors [14, 72, 73] assessing dosimetric comparisons of 177Lu-DOTATATE distributions.

3.2.1. LND-D_{SPECT} versus MC-D_{True}

The MC-D_{True} values were generally marginally lower than those obtained from LND-DSPECT, following the same trend of the highest and lowest absorbed doses seen in the tumours and liver. The absolute difference between the MC-D_{True} and the LND-D_{SPECT} for the average values

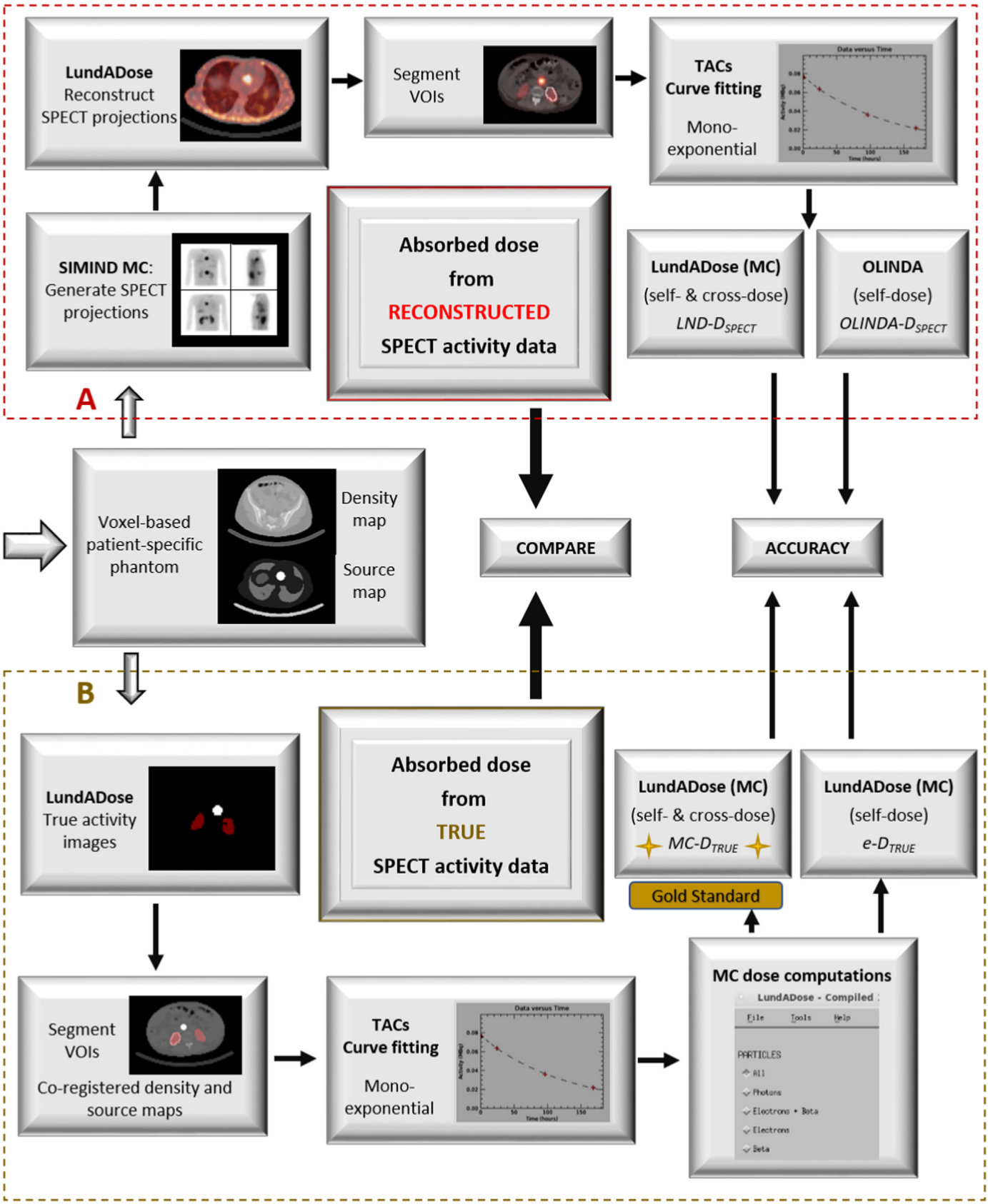

Figure 3. Schematic flow chart showing the steps followed to determine the dosimetry accuracy between the reconstructed SPECT data (A) and the true activity data (B).

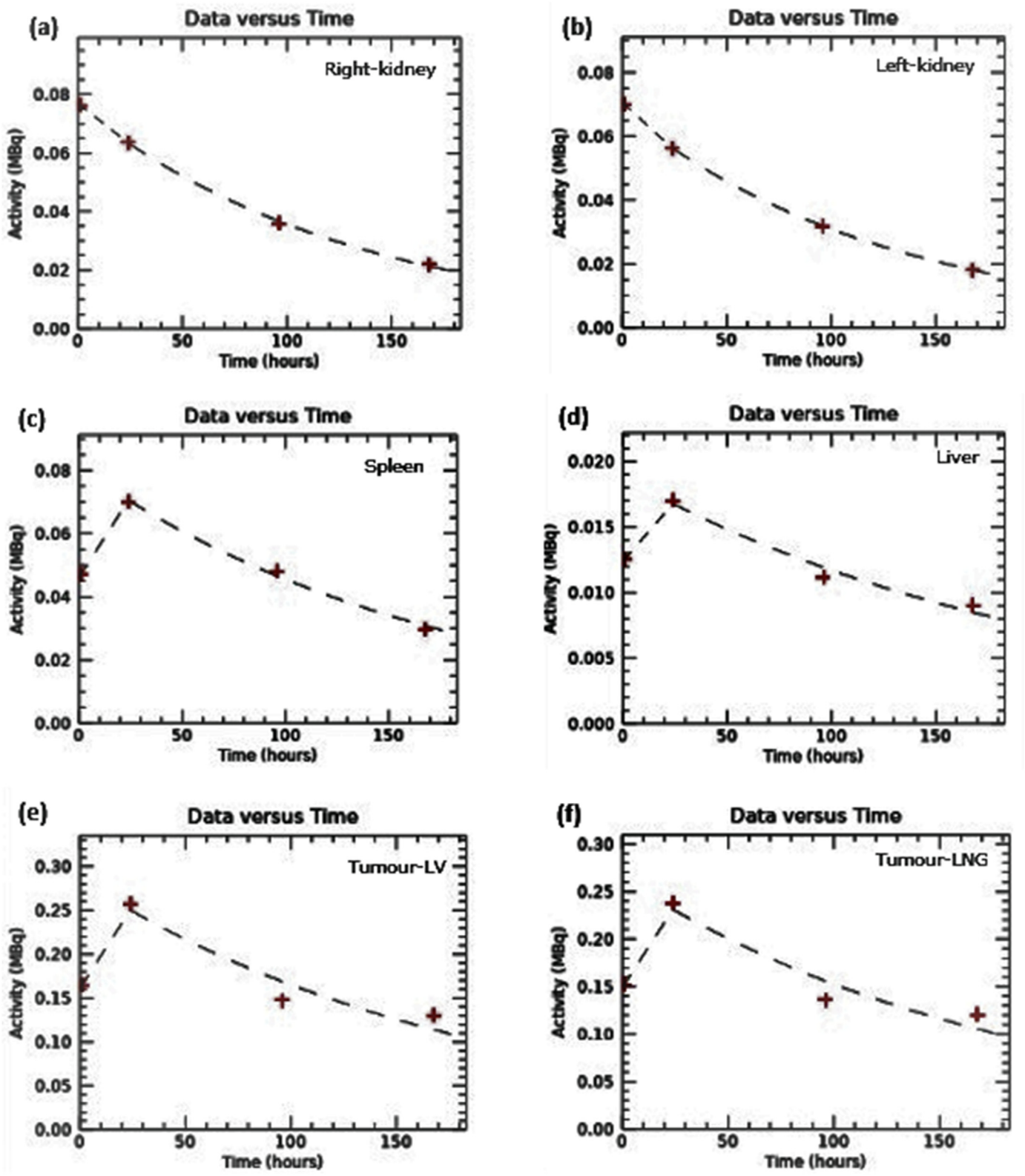

Figure 4. Examples of time activity fits obtained from the reconstructed SPECT images, used to calculate time-integrated activity for the (a) right-kidney, (b) left-kidney, (c) spleen, (d) liver, (e) tumour-LV (tumour adjacent to the liver) and (f) tumour-LNG (tumour between the lungs).

showed an overestimation by the LND-D_{SPECT} of $\geq$0.75 mGy/MBq. The dosimetry accuracy (Equation 2) of the mean absorbed doses for the LND-D_{SPECT} versus MC-D_{True} are summarised in Table 4 for the three patient phantoms. In general, the results present an overestimation of the mean absorbed dose by LND-D_{SPECT} compared to the MC-D_{True} with an accuracy better than 6.6%. The observed differences followed those seen with the TIA, with the highest accuracy observed for the spleen of phantom 2 with an inter-phantom variability of $\leq 4.4 \pm 2.2\%$, which was of the same order magnitude as the intra-organ variability of $\leq 4.4 \pm 1.8\%$.

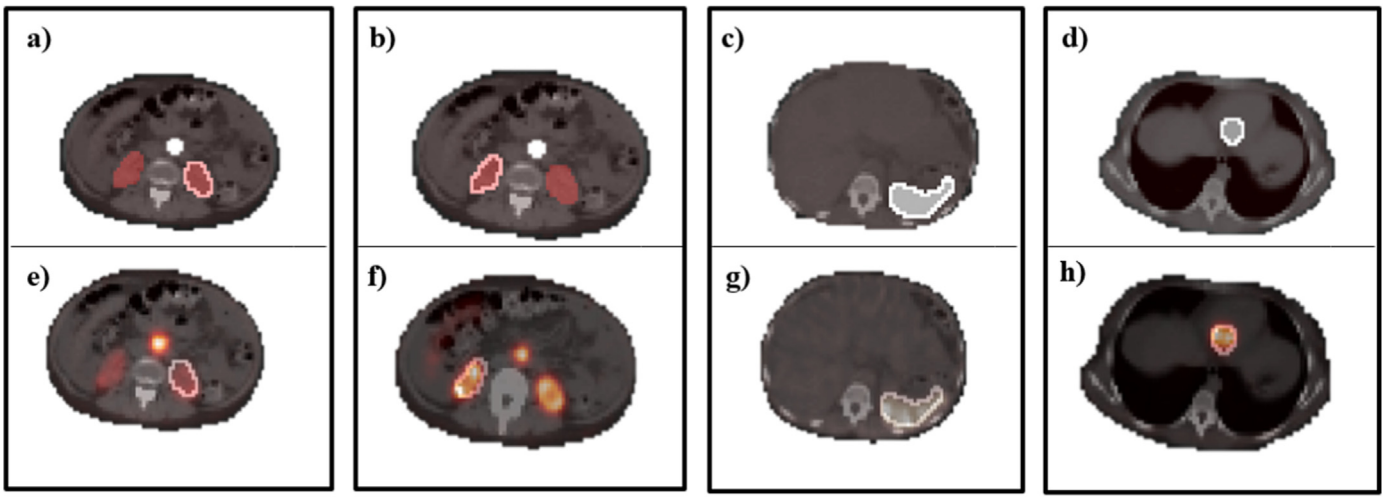

Figure 5. Example of coronal slices of the right-kidney, left-kidney, spleen, and the tumour placed between the lungs for the true activity images ((a)–(d)) and the corresponding reconstructed SPECT slices ((e)–(h)).

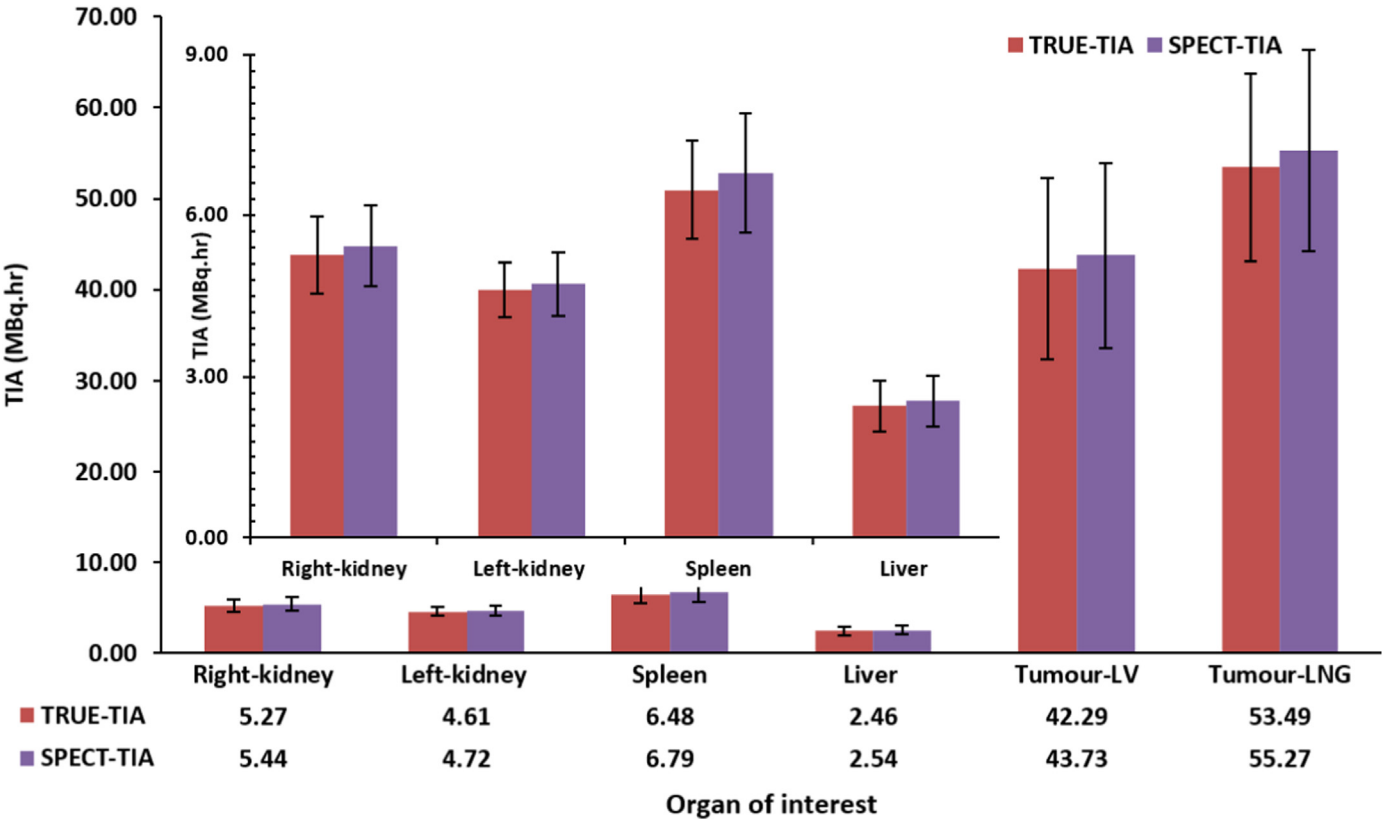

Figure 6. The average time-integrated activity (TIA) for the right-kidney, left-kidney, spleen, liver, tumour-LV (tumour adjacent to the liver), and tumour-LNG (tumour between the lungs), with a zoom-in of the data shown in the upper left section and the average of the values shown at the bottom. The TIA was computed from the true activity images (TRUE-TIA) and reconstructed SPECT images (SPECT-TIA).

3.2.2. OLINDA-D_{SPECT} versus MC-D_{True}

Similarly, the accuracies between the OLINDA-D_{SPECT} and MC-D_{True} values are presented in Table 5. The results showed a general underestimation of OLINDA-D_{SPECT} in comparison to MC-D_{True} (Figure 7). The highest accuracy was observed for the right ($\leq$6.7%) and left kidneys ($\leq$8.1%) of phantom 3, where the inter-phantom and intra-organ variability were of the same order magnitude, $\leq$ 5.6 $\pm$ 2.2%, and $\leq$5.2 $\pm$ 2.8%, respectively.

3.2.3. OLINDA-D_{SPECT} versus e-D_{True}

To show the effect of comparing true dose with MC electron self-dose versus true dose with full MC cross-dose plus self-dose, OLINDA-D_{SPECT} was compared to e-D_{True} with the percentage differences summarised in Table 6 for the three patient phantoms. The inter-phantom and intra-organ accuracy variability of $\leq$2.9 $\pm$ 2.0% and $\leq$2.9 $\pm$ 2.1%, compared marginally better than those obtained from Table 5 with corresponding values of $\leq$5.6 $\pm$ 2.2%, and $\leq$5.2 $\pm$ 2.6%. The

Table 3. The accuracy of the time-integrated activity (TIA) from the reconstructed SPECT images (SPECT-TIA) versus the TIA from the true images (TRUE-TIA) of the three phantoms for the kidneys, spleen, liver, tumour-LV (tumour adjacent to the liver) and tumour-LNG (tumour between the lungs).

	SPECT-TIA versus TRUE-TIA Accuracy (%)			
Organ	Phantom 1	Phantom 2	Phantom 3	Average
Right-kidney	1.7	3.3	4.6	3.2 ± 1.5
Left-kidney	1.3	3.9	1.9	2.4 ± 1.4
Spleen	3.5	7.2	3.2	4.6 ± 2.2
Liver	2.5	3.0	5.3	3.6 ± 1.5
Tumour-LV	3.4	2.3	4.8	3.5 ± 1.3
Tumour-LNG	4.3	2.8	2.6	3.2 ± 0.9
Average	2.8 ± 1.2	3.8 ± 1.8	3.7 ± 1.4	

Table 4. The accuracy of the mean absorbed doses computed in LundADose with full Monte Carlo (MC) transport using the reconstructed SPECT images (LND-D_{SPECT}) versus the true activity images (MC-D_{True}) of the three phantoms for the kidneys, spleen, liver, tumour-LV (tumour adjacent to the liver) and tumour-LNG (tumour between the lungs).

	LND-D_{SPECT} versus MC-D_{True} Accuracy (%)			
Organ	Phantom 1	Phantom 2	Phantom 3	Average
Right-kidney	4.4	4.0	5.6	4.7 ± 0.8
Left-kidney	2.6	5.6	1.8	3.3 ± 2.0
Spleen	4.3	6.6	2.3	4.4 ± 2.2
Liver	4.8	2.9	4.8	4.2 ± 1.1
Tumour-LV	1.5	1.8	4.8	2.7 ± 1.8
Tumour-LNG	5.6	5.4	5.5	5.5 ± 0.1
Average	3.9 ± 1.5	4.4 ± 1.8	4.1 ± 1.7	

absolute differences between the average values obtained in Table 5 and Table 6 presented an overall improved accuracy for e-D_{True} (up to 4.7% when considering the tumour next to the liver). These results suggest that the difference in the accuracy obtained by considering only self-dose by electrons was less than 5% across all the phantoms. Table 6 showed an overall improvement in the underestimations reported in Table 5.

Globally, the higher mean absorbed dose by the spleen was indicative of the increased ^{177}Lu-DOTATATE uptake compared to the other OAR. The kidney-to-tumour mean absorbed dose ratio was, on average 1:11. The absolute differences between the average values obtained amongst the three phantoms for the two tumour locations were, 2.56 mGy/MBq, 3.02 mGy/MBq, 2.45 mGy/MBq and 2.20 mGy/MBq for the MC-D_{True}, LND-D_{SPECT}, OLINDA-D_{SPECT} and e-D_{True}, respectively. Altogether, the better than 10% dose accuracy for all the data (Tables 4, 5, and 6) suggests that the mean dose values obtained with LND-D_{SPECT} and OLINDA-D_{SPECT} approximate the true values. The mean absorbed dose values between the two software programs and the gold standard compared favourably.

4. Discussion

4.1. Time-integrated activity

Different fitting models have been used to describe the evolution of activity distribution over time in organs of interest for ^{177}Lu-DOTATATE. These include: mono-exponential [3, 7, 17, 66, 67, 74], bi-exponential [47], trapezoidal integration and tri-exponential time-integrated fits for three measured time-points [75]. A mono-exponential or a bi-exponential fit is often used to integrate the TAC for ^{177}Lu-DOTATATE

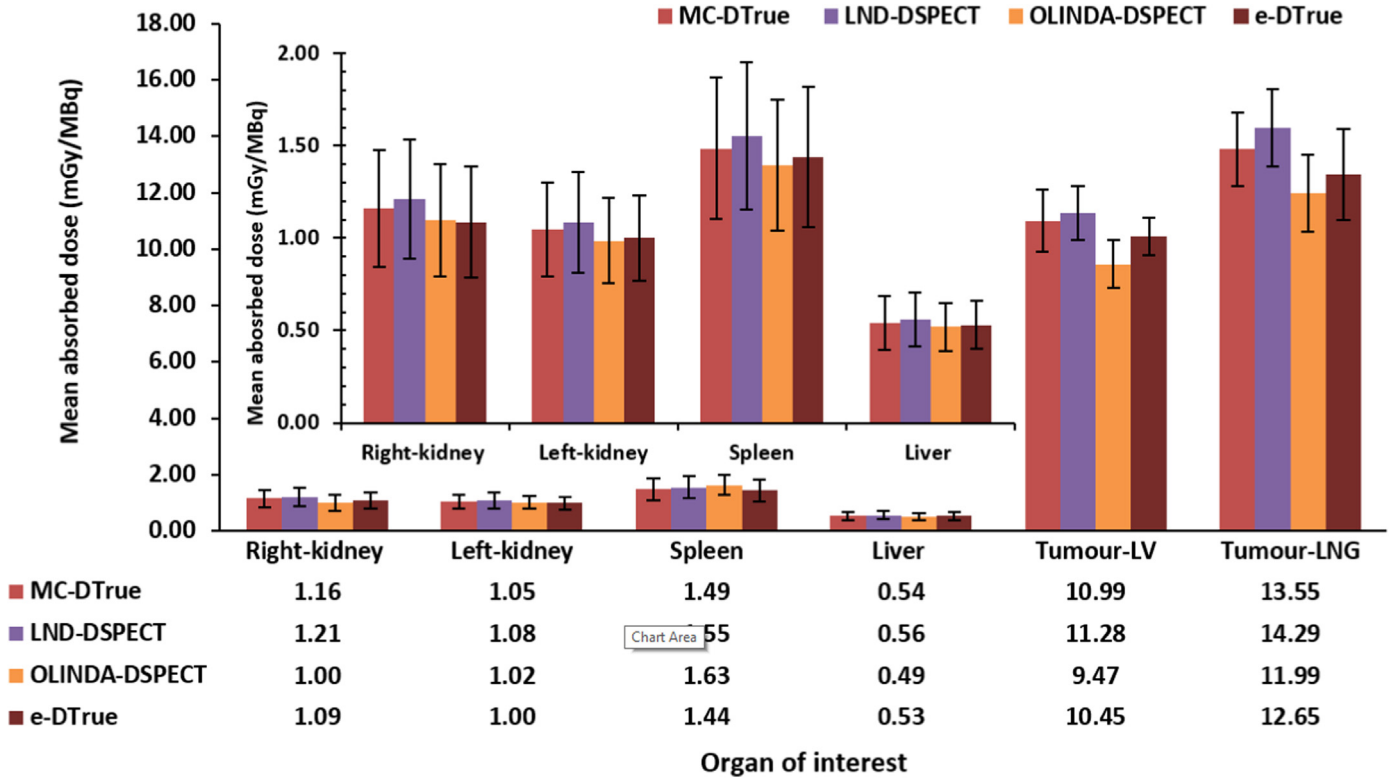

Figure 7. The mean absorbed doses for the right-kidney, left-kidney, spleen, liver and tumour-LV (tumour adjacent to the liver) and tumour-LNG (tumour between the lungs) with a zoom-in of the data shown in the upper left section and the average values shown at the bottom. Doses were computed from the true activity images using full Monte Carlo (MC) transport (MC-D_{True}) and assuming electron self-dose (e-D_{True}), as well as from reconstructed SPECT images using LundADose (LND-D_{SPECT}) and OLINDA/EXM 1.0 (OLINDA-D_{SPECT}).

Table 5. The accuracy of the mean absorbed doses computed in OLINDA using the reconstructed SPECT images (LND-D_{SPECT}) versus the mean absorbed doses computed in LundADose with full Monte Carlo (MC) transport using the true activity images (MC-D_{True}) of the three phantoms for the kidneys, spleen, liver, tumour-LV (tumour adjacent to the liver) and tumour-LNG (tumour between the lungs).

	OLINDA-D_{SPECT} versus MC-D_{True} Accuracy (%)			
Organ	Phantom 1	Phantom 2	Phantom 3	Average
Right-kidney	-5.2	-4.6	-6.7	-5.5 ± 1.1
Left-kidney	-3.9	-4.8	-8.1	-5.6 ± 2.2
Spleen	-5.3	-6.3	-6.3	-6.0 ± 0.6
Liver	-3.1	-5.7	-1.2	-3.3 ± 2.3
Tumour-LV	-6.6	-5.4	-2.9	-5.0 ± 1.9
Tumour-LNG	-4.5	-4.1	-6.2	-4.9 ± 1.1
Average	-4.8 ± 1.2	-5.2 ± 0.8	-5.2 ± 2.6	

Table 6. The accuracy of the mean absorbed doses computed in OLINDA using the reconstructed SPECT images (LND-D_{SPECT}) versus the mean absorbed doses computed in LundADose assuming self-dose from electrons using the true activity images (e-D_{True}), of the three phantoms for the kidneys, spleen, liver, tumour-LV (tumour adjacent to the liver) and tumour-LNG (tumour between the lungs).

	OLINDA-D_{SPECT} versus e-D_{True} Accuracy (%)			
Organ	Phantom 1	Phantom 2	Phantom 3	Average
Right-kidney	0.4	1.2	0.8	0.8 ± 0.4
Left-kidney	-1.3	-0.1	-2.9	-1.4 ± 1.4
Spleen	-2.0	-1.4	-5.2	-2.9 ± 2.0
Liver	-0.7	-1.2	-3.9	-1.9 ± 1.7
Tumour-LV	2.3	-0.9	-2.2	-0.3 ± 2.3
Tumour-LNG	2.7	-0.3	-3.7	-0.4 ± 3.2
Average	0.2 ± 1.9	-0.5 ± 1.0	-2.9 ± 2.1	

RPT [14]. Various fitting functions, available with LundADose, were appropriate to fit the data presented in Figure 4, including a mono-exponential, bi-exponential and quadratic exponential. In addition, there is an automatic option available in LundADose to assess the best fitting model. Although not explicitly investigated in this work, both options for automatic fit and mono-exponential fits were explored for the tumour data and resulted in equivalent values for the cumulated activity. A high target to non-target ratio characterised these curves with the highest accumulation of activity in the tumours, followed by the spleen, kidneys, and liver, respectively. The bio-kinetic profile was in agreement with ^{177}Lu-DOTATATE accumulation observed by other authors [51, 73].

LundADose included all steps required in the clinical dosimetry chain and was our reference software program in this comparison. Since our objective was to evaluate the dosimetry accuracy focussing on the absorbed dose calculation step, the same SPECT-TIAs computed from LundADose were used to compute absorbed doses in OLINDA. We followed this approach to reduce the software's variations and discrepancies in pre-preliminary steps regarding CFs, reconstruction, registration, segmentation, organs' volume determination for segmentation, TACs, and the curve fitting to obtain TIA. In this way, we could solely evaluate the dose computation step's accuracy. Since the data was obtained from voxel-based patient phantoms, much of the error propagation from factors such as activity decay and VOI definitions (contouring) was eliminated. The primary source of the error could be attributed to the poor resolution of the reconstructed SPECT images. However, this may be different when considering other clinical software that may not incorporate most of the dosimetry steps, and the above factors may contribute to the error propagation. In this case, a method is needed to assess the methodology's performance applied in each step. Furthermore, each step's uncertainty and propagation to calculate the absorbed doses should be evaluated.

Considering only the OAR, the average cumulated activity concentrations were the highest for the spleen, followed by the kidneys and the liver, as observed by Grimes [43], and Mora Ramirez et al. [14] who compared the absorbed dose computed by different dosimetry software programs. The largest variation in the TIA was found in the tumours, in agreement with Grimes [43], who mainly compared dose estimates from OLINDA, the voxel S value technique, and MC simulations for ^{177}Lu, ^{131}I and ^{90}Y. The average percentage difference of 4.6 ± 2.2% (Figure 6) amongst the phantoms was acceptable. Overall, the comparable results obtained by the TRUE-TIA and SPECT-TIA indicated that the SPECT-TIA was reliable in estimating true absorbed dose values.

4.2. Mean absorbed dose estimates

This study is phantom-based, hence our subject number seemed reasonably in line with digital phantoms' investigations and comparative studies on dosimetry software programs. Brolin et al. [49] used three pharmacokinetic digital phantoms from the XCAT generation to assess the dosimetry accuracy of ^{177}Lu-DOTATATE. Also, Mora-Ramirez et al. [14] compared commercial dosimetry software programs using only two patients during two cycles of ^{177}Lu-DOTATATE RPT. The similarity in the trend observed between the TIA and the mean absorbed doses was in agreement with findings by Mora-Ramirez et al. [14]. Most of our mean absorbed dose estimates agreed with those reported by other authors (Table 2). For example, in the case of the kidneys, our dose estimates equal to 1.16 ± 0.31 mGy/MBq, 1.21 ± 0.32 mGy/MBq, 1.10 ± 0.31 mGy/MBq and 1.09 ± 0.30 mGy/MBq computed for MC-D_{True}, LND-D_{SPECT}, OLINDA-D_{SPECT} and e-D_{True} respectively, were comparable to those indicated in Table 2 [46, 47, 48]. The large range of the kidney mean absorbed dose estimates by Sandström et al. [50], who used 777 patients in their study, indicates the dose range that may be found when considering an extensive range of patients. Kidney dosimetry has been comprehensively researched in the last decade [15, 72, 76, 77, 78], and still, there is no final consensus on how to conduct dosimetry for the kidneys. The highlight from the different methods was that planar images overestimate the quantified activity due to organ overlap, which artificially increases the kidney absorbed dose. This may be overcome by using SPECT images for activity quantification adjustment in the hybrid WB/SPECT method. Ex-vivo radiography studies of the kidneys have confirmed that the limited spatial resolution of SPECT/CT or PET/CT data does not support the segmentation of the kidney sub-regions [79]. For this reason, CT data has been well adopted as a standard method used to segment the kidney as a single structure and therefore used in this work.

Our spleen doses of 1.49 ± 0.38 mGy/MBq, 1.55 ± 0.40 mGy/MBq, 1.40 ± 0.35 mGy/MBq, and 1.44 ± 0.38 mGy/MBq obtained with MC-D_{True}, LND-D_{SPECT}, OLINDA-D_{SPECT} and e-D_{True}, respectively, were comparable to previous reports listed in Table 2. The spleen doses were often higher than those by the other organs (Figure 7), which corresponded to their higher increased uptake indicated in the TIA. In the case of the liver, our corresponding computations of 0.54 ± 0.14 mGy/MBq, 0.56 ± 0.14 mGy/MBq, 0.52 ± 0.13 mGy/MBq, and 0.53 ± 0.13 mGy/MBq were similar to those published in literature [14, 80]. The tumour doses of 13.55 ± 1.31 mGy/MBq, 14.29 ± 1.37 mGy/MBq, 12.89 ± 1.36 mGy/MBq, and 12.65 ± 1.61 mGy/MBq, obtained with MC-D_{True}, LND-D_{SPECT}, OLINDA-D_{SPECT} and e-D_{True}, agreed favourably with those listed in the existing publications (Table 2). Our tumour uptake of eleven-fold that of the dose-limiting kidneys implied the potential of delivering ideal high therapeutic doses to the tumours and lower doses to the critical organs. We considered relatively large organs i.e., the kidneys, spleen, liver, and tumours of volume 33.5 ml, to decrease any residual PVEs due to spill out. The tumour volume we used was in the same range as Grimes [43], who used three tumours ranging in size from 23 ml to 95 ml to compare internal dosimetry estimates using OLINDA, a voxel S value technique, and MC simulations.

We followed a modular approach to have the input of the reconstructed SPECT data up until the fitting of the TIA curves to be the same

for both LundADose and OLINDA. Our dosimetry accuracy was assessed by comparing these results with those computed from the true activity images. Overall, the two software programs produced dosimetry accuracy results that were comparable (Tables 4, 5, and 6) between the MC-D_{True} and LND-D_{SPECT} ($\leq 4.4 \pm 2.2\%$) and MC-D_{True} and OLINDA-D_{SPECT} ($\leq 5.6 \pm 2.2\%$) for the three phantoms. The comparable dose estimates between LND-D_{SPECT} and OLINDA-D_{SPECT} suggest that the preliminary steps' variability and compounding uncertainty between the two software programs might have been reduced. Mora-Ramirez et al. [14] presented a comparison of dosimetry results from five commercial software programs using the same TIA data and found that the dose computation step did not have a major impact on the mean absorbed doses at an organs tissue level [81]. Our findings might have to be revised when considering voxel-based dosimetry and dose-volume histograms, which offer better discrimination for the radiation transport. OLINDA assumes a uniform organ activity distribution i.e., it does not account for non-homogeneous activity uptake, and therefore our reporting of organ-level dosimetry does not reflect the impact of this non-uniform dose distribution.

The underestimation of the absorbed doses by OLINDA compared to the true doses may be attributed to the differences in the geometry between the voxel-based phantoms used in this study and the geometric reference phantoms used in OLINDA. Although the differences in the organs' masses between our phantoms and models by OLINDA are accounted for by normalising the OLINDA organs masses to ours, this does not account for the geometric differences in shape. In comparing dose calculations between OLINDA and patient-specific MC dose calculations, Grimes (2013) found that even with considerable anatomy differences between patients, mean dose estimates reported on an organ level were in good agreement between OLINDA and MC doses. Bearing in mind that the VOI delineation was in accordance with the CT data, the overestimations by LND-D_{SPECT} compared to MC-D_{True} may be attributed to the PVE. Even though PVC was applied to the quantified activity by numerical compensation using RCs in the LND-D_{SPECT} computation, it did not account for the spill-out activity outside the VOI border delineation by the CT images. This spill-out activity from the reconstructed SPECT images (LND-D_{True}) can result in dose contribution to tissue inside the VOI and offers a possible explanation for the higher dose estimates (LND-D_{True}) compared to the true doses (MC-D_{True}).

Cross-organ dose contributions are higher for more penetrating gamma rays emitted at higher intensities, such as those for ^{131}I with an energy of 364.5 keV (83.0%), compared to the ^{177}Lu 208.4 keV (10.4%). ^{177}Lu thus exhibits a lower probability of depositing energy in target organs further away from the source organ. Furthermore, due to the limited electron maximum energy of 177 keV (11.6%), 385 (9.1%), 498 keV (79.3%), the pathway for the ^{177}Lu energy depositing electrons is short in soft tissue, and thus the mean absorbed dose would be primarily due to self-dose. On average, the accuracy calculated using e-D_{True} instead of MC-D_{True} resulted in a 5% improvement. Our findings were on par with those of [80], who compared mean absorbed doses obtained with the PDOSE dosimetry toolkit with mean absorbed doses calculated by OLINDA for OAR in 21 patients who underwent ^{177}Lu-DOTATATE RPT. The authors found a 5% relative difference between the two software programs for all OAR except for the kidneys showing a 6.5% difference. The authors attributed the different kidney estimates between PDOSE and OLINDA to the fact that the right and left kidneys were considered separately for PDOSE. In contrast, OLINDA considers the kidneys as a single organ, which affects the bio-kinetic data.

Our study showed a dosimetry accuracy smaller than and equal to 6.6% using the LundADose software (Table 4: LND-D_{SPECT} with the highest difference obtained in the spleen of phantom 2) comparable to the results reported by Santoro et al. [80]. LundADose considered the kidneys separately, therefore, the reason mentioned above for the higher accuracy found for the kidneys may be extended to our study where the largest absorbed dose underestimation of 8.1% (Table 5) was seen for the left kidney of phantom 3 using OLINDA-D_{SPECT}. Grimes [43], compared dose estimates by OLINDA with MC techniques using six patients and concluded that although the anatomy may vary between the six patients and the models used in OLINDA, the mean organ dose estimates between OLINDA and MC were in good agreement (−6.2%). The overall accuracy of less than 10%, acceptable by other authors conducting similar investigations [43, 81], was reasonable between the two software programs investigated in this work.

5. Conclusion

We presented a comparison of dosimetry results generated by LundADose and OLINDA with reference to true doses with full MC transport. The accuracy of the dose estimates showed overestimations by LundADose ($\leq$6.6%) and underestimations by OLINDA ($\leq$8.1%) compared to the true doses. Our accuracy results of better than 10% were satisfactory, and our mean absorbed doses to the OAR and tumours for both software programs were concordant with literature findings. This work suggests that standardising the crucial preliminary steps in the dosimetry chain, from the gamma camera calibration process up to and including the determination of the TIA data, offers the potential to obtain comparable dose estimates between LundADose, and OLINDA for ^{177}Lu voxel-based patient-specific phantoms.

Indeed, several aspects in our study may contribute to the satisfactory accuracy and the favourable comparison obtained between LundADose and OLINDA. These approximations and limitations would need to be addressed in the application to patient data, which were not available at the time of the study. Since the study is based on virtual dosimetry using MC and voxel-based phantoms, quantities such as true activity and segmented volumes were known. These quantities would be unknown in real patients. The number of patient phantoms was relatively small and sufficient for an initial comparative phantom study. This study was performed as preliminary work that may be extended to clinical data. Currently, our clinic does not perform ^{177}Lu-DOTATATE patient RPT. The dosimetry comparison should include more diverse patient phantoms with different bio-kinetic data as part of a follow-up study. These will be available from an in-house clinical database once ^{177}Lu-DOTATATE patients are imaged routinely in our clinic.

Ethics approval and consent to participate

This study was performed with approval from the Health Sciences Research Ethics Committee at the University of the Free State (UFS), Ethics number UFS-HSD2019/1506/0110. The HSREC functions in compliance with, but not limited to, the following documents and guidelines: The SA National Health Act. No. 61 of 2003; Ethics in Health Research: Principles, Structures and Processes (2015); SA GCP(2006); Declaration of Helsinki; The Belmont Report; The US Office of Human Research Protections 45 CFR 461 (for non-exempt research with human participants conducted or supported by the US Department of Health and Human Services- (HHS), 21 CFR 50, 21 CFR 56; CIOMS; ICH-GCP-E6 Sections 1–4; The International Conference on Harmonization and Technical Requirements for Registration of Pharmaceuticals for Human Use (ICH Tripartite), Guidelines of the SA Medicines Control Council as well as Laws and Regulations concerning the Control of Medicines, Constitution of the HSREC of the Faculty of Health Sciences at UFS.

Declarations

Author contribution statement

Keamogetswe Ramonaheng: Conceived and designed the experiments; Performed the experiments; Analyzed and interpreted the data; Contributed to the analysis tools data; Wrote the paper.

Johannes A. van Staden, Hanlie du Raan: Conceived and designed the experiments; Contributed to the analysis of the data and revised the paper.

Funding statement

This work was supported by the Science and Technology Research Collaboration between the National Research Foundation of South Africa (NRF), and the Swedish Foundation for International Cooperation in Research and Higher Education (STINT), grant STINT 160811184621. Partial financial support was received from NTeMBI (Necsa).

Data availability statement

Data included in article/supp. material/referenced in article.

Declaration of interests statement

The authors declare no conflict of interest.

Additional information

No additional information is available for this paper.

Acknowledgements

The authors acknowledge the Department of Nuclear Medicine at Universitas Academic Hospital in Bloemfontein, FreeState, South Africa, for permission to use the equipment. We wish to express our gratitude to Prof. Michael Ljungberg and Prof. Katarina Sjögreen-Gleisner from the Department of Medical Radiation Physics at the University of Lund, Sweden, for making the Lundadose dosimetry software freely available to us and for their technical support. We also express our appreciation to Ms. M. Morphis for all her technical assistance with the software.

References

[1] R.L. Wahl, S. Ahuja, B. Clarke, Current landscape of radiopharmaceutical therapies: SNMMI therapy task force survey, J. Nucl. Med. Off. Publ. Soc. Nucl. Med 62 (5) (2021 May 10) 11N–16N.

[2] A. Dash, M.R.A. Pillai, F.F. Knapp, Production of ^{177}Lu for targeted radionuclide therapy: available options, Nucl. Med. Mol. Imaging 49 (2) (2015 Jun) 85–107.

[3] L. Bodei, M. Cremonesi, M. Ferrari, M. Pacifici, C.M. Grana, M. Bartolomei, et al., Long-term evaluation of renal toxicity after peptide receptor radionuclide therapy with ^{90}Y-DOTATOC and ^{177}Lu-DOTATATE: the role of associated risk factors, Eur. J. Nucl. Med. Mol. Imag. 35 (10) (2008 Oct) 1847–1856.

[4] A.T. Kendi, T.R. Halfdanarson, A. Packard, A. Dundar, R.M. Subramaniam, Therapy with ^{177}Lu-DOTATATE: clinical implementation and impact on care of patients with neuroendocrine tumors, Am. J. Roentgenol. 213 (2) (2019 Aug 1) 309–317.

[5] D.J. Kwekkeboom, W.W. de Herder, B.L. Kam, C.H. van Eijck, M. van Essen, P.P. Kooij, et al., Treatment with the radiolabeled somatostatin analog [^{177}Lu-DOTA 0,Tyr3]octreotate: toxicity, efficacy, and survival, J. Clin. Oncol. Off. J. Am. Soc. Clin. Oncol 26 (13) (2008 May 1) 2124–2130.

[6] J. Smith-Palmer, O.R. Leeuwenkamp, J. Virk, N. Reed, Lutetium oxodotreotide (^{177}Lu-Dotatate) for the treatment of unresectable or metastatic progressive gastroenteropancreatic neuroendocrine tumors: a cost-effectiveness analysis for Scotland, BMC Cancer 21 (1) (2021 Jan 5) 10.

[7] L. Bodei, M. Cremonesi, C.M. Grana, N. Fazio, S. Iodice, S.M. Baio, et al., Peptide receptor radionuclide therapy with ^{177}Lu-DOTATATE: the IEO phase I-II study, Eur. J. Nucl. Med. Mol. Imag. 38 (12) (2011 Dec) 2125–2135.

[8] J. Kunikowska, L. Królicki, A. Hubalewska-Dydejczyk, R. Mikołajczak, A. Sowa-Staszczak, D. Pawlak, Clinical results of radionuclide therapy of neuroendocrine tumours with ^{90}Y-DOTATATE and tandem ^{90}Y/^{177}Lu-DOTATATE: which is a better therapy option? Eur. J. Nucl. Med. Mol. Imag. 38 (10) (2011 Oct) 1788–1797.

[9] J. Strosberg, G. El-Haddad, E. Wolin, A. Hendifar, J. Yao, B. Chasen, et al., Phase 3 trial of ^{177}Lu-dotatate for midgut neuroendocrine tumors, N. Engl. J. Med. 376 (2) (2017) 125–135, 12.

[10] L. Villard, A. Romer, N. Marincek, P. Brunner, M.T. Koller, C. Schindler, et al., Cohort study of somatostatin-based radiopeptide therapy with [^{90}Y-DOTA]-TOC versus [^{90}Y-DOTA]-TOC plus [^{177}Lu-DOTA]-TOC in neuroendocrine cancers, J. Clin. Oncol. Off. J. Am. Soc. Clin. Oncol 30 (10) (2012 Apr 1) 1100–1106.

[11] E. Ilan, M. Sandström, C. Wassberg, A. Sundin, U. Garske-Román, B. Eriksson, et al., Dose response of pancreatic neuroendocrine tumors treated with peptide receptor radionuclide therapy using ^{177}Lu-DOTATATE, J. Nucl. Med. Off. Publ. Soc. Nucl. Med 56 (2) (2015 Feb) 177–182.

[12] M. Lassmann, U. Eberlein, Radiation dosimetry aspects of ^{177}Lu, Curr. Rad. 8 (2) (2015) 139–144.

[13] M. Bardiès, J.I. Gear, Scientific developments in imaging and dosimetry for molecular radiotherapy, Clin. Oncol. R. Coll. Radiol. G. B 33 (2) (2021 Feb) 117–124.

[14] E. Mora-Ramirez, L. Santoro, E. Cassol, J.C. Ocampo-Ramos, N. Clayton, G. Kayal, et al., Comparison of commercial dosimetric software platforms in patients treated with ^{177}Lu-DOTATATE for peptide receptor radionuclide therapy, Med. Phys. 47 (9) (2020 Sep) 4602–4615.

[15] M. Larsson, P. Bernhardt, J.B. Svensson, B. Wängberg, H. Ahlman, E. Forssell-Aronsson, Estimation of absorbed dose to the kidneys in patients after treatment with ^{177}Lu-octreotate: comparison between methods based on planar scintigraphy, EJNMMI Res. 2 (1) (2012 Sep 24) 49.

[16] Y. Dewaraja, S. Wilderman, J. Niedbala, K. Frey, K.K. Wong, Multi SPECT/CT-based patient specific lesion and kidney dosimetry for verification of simpler approaches for treatment planning in Lu-177 DOTATATE PRRT, J. Nucl. Med. 60 (supplement 1) (2019 May 1) 1626.

[17] A. Sundlöv, K. Sjögreen-Gleisner, J. Svensson, M. Ljungberg, T. Olsson, P. Bernhardt, et al., Individualised ^{177}Lu-DOTATATE treatment of neuroendocrine tumours based on kidney dosimetry, Eur. J. Nucl. Med. Mol. Imag. 44 (9) (2017 Aug) 1480–1489.

[18] P.B. Zanzonico, Internal radionuclide radiation dosimetry: a review of basic concepts and recent developments, J. Nucl. Med. Off. Publ. Soc. Nucl. Med 41 (2) (2000 Feb) 297–308.

[19] W.E. Bolch, K.F. Eckerman, G. Sgouros, S.R. Thomas, MIRD pamphlet No. 21: a generalized schema for radiopharmaceutical dosimetry–standardization of nomenclature, J. Nucl. Med. Off. Publ. Soc. Nucl. Med 50 (3) (2009 Mar) 477–484.

[20] R. Loevinger, T.F. Budinger, E.E. Watson, Mird Primer for Absorbed Dose Calculations. Revised, Subsequent edition, Society of Nuclear Medicine, New York, NY, 1991.

[21] G. Glatting, P. Kletting, S.N. Reske, K. Hohl, C. Ring, Choosing the optimal fit function: comparison of the Akaike information criterion and the F-test, Med. Phys. 34 (11) (2007 Nov) 4285–4292.

[22] P. Kletting, S. Schimmel, H. Hänscheid, M. Luster, M. Fernández, D. Nosske, et al., The NUKDOS software for treatment planning in molecular radiotherapy, Z. Med. Phys. 25 (3) (2015 Sep) 264–274.

[23] P. Kletting, T. Kull, S.N. Reske, G. Glatting, Comparing time activity curves using the Akaike information criterion, Phys. Med. Biol. 54 (21) (2009 Nov 7) N501–507.

[24] M. Stabin, A. Farmer, OLINDA/EXM 2.0: the new generation dosimetry modeling code, J. Nucl. Med. 53 (supplement 1) (2012 May 1) 585.

[25] M.G. Stabin, MIRDOSE: personal computer software for internal dose assessment in nuclear medicine, J. Nucl. Med. Off. Publ. Soc. Nucl. Med 37 (3) (1996 Mar) 538–546.

[26] M.G. Stabin, R.B. Sparks, E. Crowe, OLINDA/EXM: the second-generation personal computer software for internal dose assessment in nuclear medicine, J. Nucl. Med. Off. Publ. Soc. Nucl. Med 46 (6) (2005 Jun) 1023–1027.

[27] A.S. Pasciak, A.C. Bourgeois, Y.C. Bradley, A comparison of techniques for ^{90}Y PET/CT image-based dosimetry following radioembolization with resin microspheres, Front. Oncol. 4 (2014 May 22) 121.

[28] A.C. Traino, M. Piccinno, C. Avigo, Dosimetry of non-uniform activity distribution: possibility to use the local energy deposition approach at the voxel level in radionuclide therapy, Biomed. Phys. Eng. Express 2 (6) (2016 Nov), 065001.

[29] A. Dieudonné, R.F. Hobbs, R. Lebtahi, F. Maurel, S. Baechler, R.L. Wahl, et al., Study of the impact of tissue density heterogeneities on 3-dimensional abdominal dosimetry: comparison between dose kernel convolution and direct Monte Carlo methods, J. Nucl. Med. Off. Publ. Soc. Nucl. Med 54 (2) (2013 Feb) 236–243.

[30] A. Dieudonné, R.F. Hobbs, W.E. Bolch, G. Sgouros, I. Gardin, Fine-resolution voxel S values for constructing absorbed dose distributions at variable voxel size, J. Nucl. Med. Off. Publ. Soc. Nucl. Med 51 (10) (2010 Oct) 1600–1607.

[31] S. Agostinelli, J. Allison, K. Amako, J. Apostolakis, H. Araujo, P. Arce, et al., Geant4—a simulation toolkit, Nucl. Instrum. Methods. Phys. Res. Sect. Accel. Spectrometers Detect. Assoc. Equip 506 (3) (2003 Jul 1) 250–303.

[32] I. Kawrakow, E. Mainegra-Hing, F. Tessier, et al., The EGSnrc Code System: Monte Carlo Simulation of Electron and Photon Transport, National Research Council Canada, Ottawa, ON, Canada, 2016.

[33] E. Larsson, M. Ljungberg, S.-E. Strand, B.-A. Jönsson, Monte Carlo calculations of absorbed doses in tumours using a modified MOBY mouse phantom for pre-clinical dosimetry studies, Acta. Oncol. Stockh. Swed. 50 (6) (2011 Aug) 973–980.

[34] M. Ljungberg, K. Sjögreen Gleisner, Personalized dosimetry for radionuclide therapy using molecular imaging tools, Biomedicines 4 (4) (2016 Nov 15) 25.

[35] L. Waters, G. Mckinney, J. Durkee, M. Fensin, J. Hendricks, M. James, et al., The MCNPX Monte Carlo radiation transport code, AIP Conf. Proc. 896 (2007 Mar 19) 81–90.

[36] D.M.V. Huizing, B.J. de Wit-van der Veen, M. Verheij, M.P.M. Stokkel, Dosimetry methods and clinical applications in peptide receptor radionuclide therapy for neuroendocrine tumours: a literature review, EJNMMI Res. 8 (2018 Aug 29) 89.

[37] E. Hippeläinen, M. Tenhunen, A. Sohlberg, Fast voxel-level dosimetry for ^{177}Lu labelled peptide treatments, Phys. Med. Biol. 60 (17) (2015 Sep 7) 6685–6700.

[38] M. Ljungberg, K. Sjögreen-Gleisner, The accuracy of absorbed dose estimates in tumours determined by quantitative SPECT: a Monte Carlo study, Acta. Oncol. Stockh. Swed. 50 (6) (2011 Aug) 981–989.

[39] W.E. Bolch, L.G. Bouchet, J.S. Robertson, B.W. Wessels, J.A. Siegel, R.W. Howell, et al., MIRD pamphlet No. 17: the dosimetry of nonuniform activity distributions–radionuclide S values at the voxel level. Medical Internal Radiation Dose Committee, J. Nucl. Med. Off. Publ. Soc. Nucl. Med. 40 (1) (1999 Jan) 11S–36S.

[40] G. Loudos, I. Tsougos, S. Boukis, N. Karakatsanis, P. Georgoulias, K. Theodorou, et al., A radionuclide dosimetry toolkit based on material-specific Monte Carlo dose kernels, Nucl. Med. Commun. 30 (7) (2009 Jul) 504–512.

[41] N. Lanconelli, M. Pacilio, S. Lo Meo, F. Botta, A. Di Dia, A.T. Aroche, et al., A free database of radionuclide voxel S values for the dosimetry of nonuniform activity distributions, Phys. Med. Biol. 57 (2) (2012 Jan 21) 517–533.

[42] M. Ljungberg, K. Sjögreen, X. Liu, E. Frey, Y. Dewaraja, S.-E. Strand, A 3-dimensional absorbed dose calculation method based on quantitative SPECT for radionuclide therapy: evaluation for ^{131}I using Monte Carlo simulation, J. Nucl. Med. Off. Publ. Soc. Nucl. Med. 43 (8) (2002 Aug) 1101–1109.

[43] J. Grimes, Patient-specific Internal Dose Calculation Techniques for Clinical Use in Targeted Radionuclide Therapy, University of British Columbia, 2013.

[44] A. Denis-Bacelar, S. Chittenden, A. Divoli, J. Gear, G. Flux, qDose, a 3D treatment planning system for molecular radiotherapy, in: EANM conference. Conference record, Milan, Italy 39, 2012, p. S351 (2).

[45] D. Villoing, M.-P. Garcia, F. Botta, S. Brillouet, F. Courbon, M. Cremonesi, et al., DosiTest: a virtual intercomparison of clinical dosimetry trials in nuclear medicine based on Monte Carlo modeling, Phys. Medica. Eur. J. Med. Phys. 30 (2014 Dec 1) e134.

[46] M. Garkavij, M. Nickel, K. Sjögreen-Gleisner, M. Ljungberg, T. Ohlsson, K. Wingårdh, et al., ^{177}Lu-[DOTA0,Tyr3] octreotate therapy in patients with disseminated neuroendocrine tumors: analysis of dosimetry with impact on future therapeutic strategy, Cancer 116 (4 Suppl) (2010 Feb 15) 1084–1092.

[47] G. Marin, B. Vanderlinden, I. Karfis, T. Guiot, Z. Wimana, N. Reynaert, et al., A dosimetry procedure for organs-at-risk in ^{177}Lu peptide receptor radionuclide therapy of patients with neuroendocrine tumours, Phys. Med. 56 (2018 Dec 1) 41–49.

[48] M. Nickel, M. Ljungberg, K. Sjogreen-Gleisner, A comparison of different image-based methods for kidney dosimetry in patients treated with ^{177}Lu-DOTATATE, J. Nucl. Med. 50 (supplement 2) (2009 May 1) 501.

[49] G. Brolin, J. Gustafsson, M. Ljungberg, K.S. Gleisner, Pharmacokinetic digital phantoms for accuracy assessment of image-based dosimetry in^{177}Lu-DOTATATE peptide receptor radionuclide therapy, Phys. Med. Biol. 60 (15) (2015 Jul) 6131–6149.

[50] M. Sandström, N. Freedman, K. Fröss-Baron, T. Kahn, A. Sundin, Kidney dosimetry in 777 patients during ^{177}Lu-DOTATATE therapy: aspects on extrapolations and measurement time points, EJNMMI Phys 7 (1) (2020 Dec 9) 73.

[51] L. Santoro, E. Mora-Ramirez, D. Trauchessec, S. Chouaf, P. Eustache, J.-P. Pouget, et al., Implementation of patient dosimetry in the clinical practice after targeted radiotherapy using [^{177}Lu-[DOTA0, Tyr3]-octreotate, EJNMMI Res. 8 (1) (2018 Nov 29) 103.

[52] S. Gupta, S. Singla, C. Bal, Patient specific dosimetry in peptide receptor radionuclide therapy of neuroendocrine tumors with ^{177}Lu-DOTATATE, J. Nucl. Med. 54 (supplement 2) (2013 May 1) 583.

[53] J. Svensson, G. Berg, B. Wängberg, M. Larsson, E. Forssell-Aronsson, P. Bernhardt, Renal function affects absorbed dose to the kidneys and haematological toxicity during ^{177}Lu-DOTATATE treatment, Eur. J. Nucl. Med. Mol. Imag. 42 (6) (2015) 947–955.

[54] D. Roth, J.R. Gustafsson, C.F. Warfvinge, A. Sundlöv, A. Åkesson, J. Tennvall, et al., Dosimetric quantities of neuroendocrine tumors over treatment cycles with ^{177}Lu-DOTA-TATE, J. Nucl. Med. Off. Publ. Soc. Nucl. Med. (2021 Jul 16), 262069 jnumed.121.

[55] M. Ljungberg, S.-E. Strand, A Monte Carlo program for the simulation of scintillation camera characteristics, Comput. Methods Progr. Biomed. 29 (4) (1989 Aug 1) 257–272.

[56] K. Ramonaheng, J.A. van Staden, H. du Raan, Validation of a Monte Carlo modelled gamma camera for Lutetium-177 imaging, Appl. Radiat. Isot. 27 (2020 Apr), 109200.

[57] P.A. Yushkevich, Y. Gao, G. Gerig, ITK-SNAP: an interactive tool for semi-automatic segmentation of multi-modality biomedical images, Conf. Proc. Annu. Int. Conf. IEEE Eng. Med. Biol. Soc. IEEE Eng. Med. Biol. Soc. Annu. Conf 2016 (2016 Aug) 3342–3345.

[58] K. Ramonaheng, J.A. van Staden, H. du Raan, The effect of calibration factors and recovery coefficients on ^{177}Lu SPECT activity quantification accuracy: a Monte Carlo study, EJNMMI Phys 8 (1) (2021 Mar 18) 27.

[59] J.A. Siegel, M.G. Stabin, Absorbed fractions for electrons and beta particles in spheres of various sizes, J. Nucl. Med. Off. Publ. Soc. Nucl. Med. 35 (1) (1994 Jan) 152–156.

[60] A. Sabet, K. Ezziddin, U.-F. Pape, K. Reichman, T. Haslerud, H. Ahmadzadehfar, et al., Accurate assessment of long-term nephrotoxicity after peptide receptor radionuclide therapy with ^{177}Lu-octreotate, Eur. J. Nucl. Med. Mol. Imag. 41 (3) (2014 Mar) 505–510.

[61] Y.K. Dewaraja, S.J. Wilderman, M. Ljungberg, K.F. Koral, K. Zasadny, M.S. Kaminiski, Accurate dosimetry in ^{131}I radionuclide therapy using patient-specific, 3-dimensional methods for SPECT reconstruction and absorbed dose calculation, J. Nucl. Med. Off. Publ. Soc. Nucl. Med. 46 (5) (2005 May) 840–849.

[62] W.R. Nelson, H. Hirayama, D.W.O. Rogers, EGS4 Code System, Stanford Linear Accelerator Center, Menlo Park, CA (USA), 1985 Dec. Report No.: SLAC-265.

[63] M. Ljungberg, K. Sjögreen Gleisner, Hybrid imaging for patient-specific dosimetry in radionuclide therapy, Diagnostics 5 (3) (2015 Jul 10) 296–317.

[64] P. Knoll, D. Kotalova, G. Köchle, I. Kuzelka, G. Minear, S. Mirzaei, et al., Comparison of advanced iterative reconstruction methods for SPECT/CT, Z. Med. Phys. 22 (1) (2012 Feb) 58–69.

[65] J. Schindelin, I. Arganda-Carreras, E. Frise, V. Kaynig, M. Longair, T. Pietzsch, et al., Fiji: an open-source platform for biological-image analysis, Nat. Methods 9 (7) (2012 Jun 28) 676–682.

[66] M. Sandström, U. Garske, D. Granberg, A. Sundin, H. Lundqvist, Individualized dosimetry in patients undergoing therapy with ^{177}Lu-DOTA-D-Phe (1)-Tyr (3)-octreotate, Eur. J. Nucl. Med. Mol. Imag. 37 (2) (2010 Feb) 212–225.

[67] C. Wehrmann, S. Senftleben, C. Zachert, D. Müller, R.P. Baum, Results of individual patient dosimetry in peptide receptor radionuclide therapy with ^{177}Lu DOTA-TATE and ^{177}Lu DOTA-NOC, Cancer Biother. Radiopharm. 22 (3) (2007 Jun) 406–416.

[68] M. Ljungberg, E. Frey, K. Sjögreen, X. Liu, Y. Dewaraja, S.-E. Strand, 3D absorbed dose calculations based on SPECT: evaluation for ^{111}In/^{90}Y therapy using Monte Carlo simulations, Cancer Biother. Radiopharm. 18 (1) (2003 Feb 1) 99–107.

[69] E.C. Frey, B.M.W. Tsui, A New method for modeling the spatially-variant, object-dependent scatter response function in SPECT, in: IEEE Nuclear Science Symposium & Medical Imaging Conference, Conference record, Anaheim, CA, USA, 1996, pp. 1082–1086.

[70] E.C. Frey, B.M.W. Tsui, A practical method for incorporating scatter in a projector-backprojector for accurate scatter compensation in SPECT, IEEE Trans. Nucl. Sci. 40 (4) (1993 Aug) 1107–1116.

[71] N.J. Begum, A. Thieme, N. Eberhardt, R. Tauber, C. D'Alessandria, A.J. Beer, et al., The effect of total tumor volume on the biologically effective dose to tumor and kidneys for ^{177}Lu-labeled PSMA peptides, J. Nucl. Med. 59 (6) (2018 Jun 1) 929–933.

[72] D.L. Bailey, T.M. Hennessy, K.P. Willowson, E.C. Henry, D.L.H. Chan, A. Aslani, et al., In vivo quantification of ^{177}Lu with planar whole-body and SPECT/CT gamma camera imaging, EJNMMI Phys 2 (1) (2015 Sep) 20.

[73] Y. Kim, J. Oh, C. Yoo, B.-Y. Ryoo, J.-S. Ryu, Prediction of absorbed dose by tumors and critical organs after Lu-177-DOTATATE therapy using pretherapeutic Ga-68-DOTATOC PET/CT, J. Nucl. Med. 62 (supplement 1) (2021 May 1) 76.

[74] W. Zhao, P.L. Esquinas, A. Frezza, X. Hou, J.-M. Beauregard, A. Celler, Accuracy of kidney dosimetry performed using simplified time activity curve modelling methods: a ^{177}Lu-DOTATATE patient study, Phys. Med. Biol. 64 (17) (2019 Aug), 175006.

[75] P.A. Jackson, M.S. Hofman, R.J. Hicks, M. Scalzo, J. Violet, Radiation dosimetry in ^{177}Lu-PSMA-617 therapy using a single posttreatment SPECT/CT scan: a novel methodology to generate time- and tissue-specific dose factors, J. Nucl. Med. 61 (7) (2020 Jul) 1030–1036.

[76] K. Willowson, H. Ryu, P. Jackson, A. Singh, E. Eslick, D. Bailey, A comparison of 2D and 3D kidney absorbed dose measures in patients receiving ^{177}Lu-DOTATATE, Asia Ocean J. Nucl. Med. Biol 6 (2) (2018) 113–119.

[77] K.P. Willowson, E. Eslick, H. Ryu, A. Poon, E.J. Bernard, D.L. Bailey, Feasibility and accuracy of single time point imaging for renal dosimetry following ^{177}Lu-DOTATATE ('Lutate') therapy, EJNMMI Phys. 5 (1) (2018) 33.

[78] J. Tran-Gia, M. Lassmann, Optimizing image quantification for Lu-177 SPECT/CT based on a 3D printed 2-compartment kidney phantom, J. Nucl. Med. (2017 Nov 2) jnumed.117.200170.

[79] A. Helisch, G.J. Förster, H. Reber, H.-G. Buchholz, R. Arnold, B. Göke, et al., Pre-therapeutic dosimetry and biodistribution of ^{86}Y-DOTA-Phe1-Tyr3-octreotide versus ^{111}In-pentetreotide in patients with advanced neuroendocrine tumours, Eur. J. Nucl. Med. Mol. Imag. 31 (10) (2004 Oct) 1386–1392.

[80] L. Santoro, L. Pitalot, D. Trauchessec, E. Mora-Ramirez, P.O. Kotzki, M. Bardiès, et al., Clinical implementation of PLANET® Dose for dosimetric assessment after [^{177}Lu]Lu-DOTA-TATE: comparison with Dosimetry Toolkit® and OLINDA/EXM® V1.0, EJNMMI Res. 11 (1) (2021 Jan 4) 1.

[81] Dosimetric estimations using commercial workstations for peptide receptor radionuclide therapy (PRRT) patients treated with 177Lu-DOTATATE, in: Conference: Annual Congress of the European Association of Nuclear Medicine, EANM, 2017.